X-ray multilens interferometer based on Si refractive lenses

A. Snigirev[1], I. Snigireva[1], M. Lyubomirskiy[1], V. Kohn[2], V. Yunkin[3], S. Kuznetsov[3]
[1] *ESRF, 38043 Grenoble, France*
[2] *Russian Research Center "Kurchatov Institute", 123182Moscow, Russia*
[3] *Institute of Microelectronics Technology RAS, 142432 Chernogolovka, Russia*

ABSTRACT

We report a multilens X-ray interferometer consisting of six parallel arrays of planar compound refractive lenses. The main concept of new interferometer is based on the same principle such a bilens interferometer. The interference fringe pattern produced by the multilens interferometer was described by Talbot imaging formalism. A theoretical analysis of the interference pattern formation was carried out and corresponding computer simulations were performed. The proposed multilens interferometer was experimentally tested at ID06 ESRF beamline in the X-ray energy range from 10 to 30 keV. Experimentally recorded fractional Talbot images are in a good agreement with computer calculations.

Keywords: X-Rays, X-Ray interferometry, Refractive lenses, Talbot effect, Planar microfabrication technology, MEMS, Standing wave.

INTRODUCTION

An evolution of X-ray sources such as third generation synchrotrons and free electron lasers led to a development and utilization of coherent methods of study. Classical optical interferometric techniques such as Young double slit interferometer [1], Fresnel bimirror [2] or a grating interferometer [3] became possible to perform in a hard X-Ray region. An idea of these set-ups is based on creating of secondary sources by non transparent narrow slits or small angle reflection by mirrors. However the field of applications of interferometers was concentrated to study of coherent properties of X-Ray sources due to low resolution of an interference pattern (standing wave) and a loss of intensity.

A new approach to creating of a small secondary source is to utilize a refractive optics [4] that is now widely used on synchrotron beamlines [5-9]. Refractive optics can be easily inserted and removed from the beam to allow fast switching of the beam size from centimeter to nanometer scale.

The field of applications of the refractive optics is not only limited by a beam conditioning and can be extended into the area of Fourier optics, coherent diffraction and imaging techniques [10-11]. Using the native property of the refractive lens as a Fourier transformer, the coherent diffraction microscopy and high resolution diffraction methods were proposed to study 3-D structures of semiconductor crystals and mesoscopic materials [12-15].

The approach to creating narrow secondary sources was demonstrated in a bilens interferometer that was recently proposed [16]. Under coherent illumination two diffraction limited secondary coherent sources are arise, the cones diverging from these sources overlap, and in this region of superposition interference occurs with a variable period ranging from tens of nanometers to tens of micrometers. This simple way to create high resolution (up to few nanometers) X-ray standing wave in paraxial geometry opens up the opportunity to develop new X-ray interferometry techniques to study natural and advanced man-made nanoscale materials, such as self-organized bio-systems, photonic and colloidal crystals, and nanoelectronics materials. As an evolution of inline bilens system in order to extend beam acceptance we propose a multilens interferometer in which more than two parallel lens arrays are arranged. The enlargement of the interferometer acceptance gives rise to the increase of the intensity and contrast of the interference fringes at the expense of narrowing of the maxima.

The bilens system produces a monotonous broadened (steadily expanded) sinusoidal interference field while multilens arrangement substantially changes the interference pattern adding strong longitudinal functional dependence. For simplicity we will describe the interference fringe pattern produced by multilens interferometer using Talbot imaging formalism [17]. It is known the object illuminated by a monochromatic plane wave can be self reproduced at

Advances in X-Ray/EUV Optics and Components IX, edited by Christian Morawe, Ali M. Khounsary, Shunji Goto, Proc. of SPIE Vol. 9207, 920703 · © 2014 SPIE
CCC code: 0277-786X/14/$18 · doi: 10.1117/12.2061616

Talbot distance $z_T = 2d^2/\lambda$, where d is grating period and λ is the wavelength of light. In case of spherical wave illumination Talbot distances are calculated by the formula $\frac{1}{z_0}+\frac{1}{z_T}=\frac{\lambda}{2d^2}$ and the distance to the source should be taken into account. It was demonstrated that there is in fact an infinite family of fractional Talbot images between the primary and secondary images [18-21]. The fractional Talbot distances are $z_{pq} = z_T\ p/q$, where p and q are small integers, such that the fraction is, e.g., (p/q) = 1/2, 1/4, 2/3. However, the main set of distances is $z_n = z_T / 2n$, where n = 1, 2, etc.

We emphasize that the classical amplitude grid in Talbot imaging is replaced by a collection of periodic line sources produced by linear lens arrays separated by the distance d. It is well to bear in mind that the Talbot distance counted from lens foci and at Talbot distances we have image of the focal lines. It should be mentioned that the Talbot imaging approach was already applied at hard X-rays. A single Fresnel diffraction image of a grating obtained with a microfocus x-ray generator in reflection geometry was described, fractional Talbot imaging of phase grating at reduced defocusing distances were used for coherence characterization and phase modulation of the object, as well as grating interferometer for phase contrast imaging [22-24].

As a proof of the concept we manufactured and tested the sixlens interferometer. It consists of six identical, parallel planar compound refractive lenses separated transversally by a distance d. The interference pattern formation was studied theoretically and computer simulations were performed. The optical properties of the interferometer were studied experimentally in the wide X-ray energy range.

2. SIXLENS INTERFEROMETER DESIGN AND MANUFACTURING

The schematic view of sixlens interferometer is shown in Figure 1. Each lens focuses the beam at a distance $z_f = F/(1-F/z_0)$, where $F = R/2N\delta$ is the lens focal length and z_0 is the source-to-lens distance, R is the radius of curvature of one parabolic surface, N is the number of double concave elements in the lens, δ is the decrement of refraction index $n = 1 - \delta + i\beta$. Under coherent illumination each lens generates a coherent, diffraction limited focal spot of size $w_f = 0.44\lambda z_f / A_{eff}$, where λ is the wavelength and $A_{eff} = 0.66(\lambda z_f \delta/\beta)^{1/2}$ is the absorption limited effective aperture of the lens [4]. At a distance $z > 3z_f d / A_{eff}$ the cones diverging from all six secondary sources overlap, and in this region interference occurs.

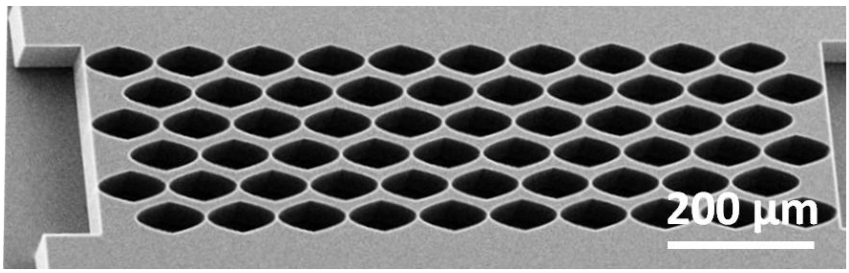

Figure 1. Scanning Electron Microscope image of the sixlens interferometer.

The sixlens interferometer was manufactured using a process involving electron beam lithography and deep etching into silicon [7, 9]. The length and aperture of each single, double concave individual lens are 62 and 30 µm respectively. Structures are 70 µm deep. The radius of the parabola apex is R = 3.75 µm, and the minimum thickness between the parabola apexes is 2 µm. The split distance between lens arrays in the interferometer is d = 30 µm. In order to obtain such small split distance and to reduce the Si transmittance at higher energies which spoil the performance of the interference fringes, we applied the new interferometer design. The novelty of the design is that lens arrays in the

interferometer are arranged in a chessboard pattern, or to put it differently arrays are shifted relative to each other by the distance equal to half length of the single individual lens. Additional advantage of such lens arrangement is the coincidence of the lens array separation period and lens physical aperture. A Scanning Electron Microscope image of the six-lens interferometer that designed for 10 keV is shown in Fig. 1. With the aim to simplify the use of interferometers in the experiments where energy tunability is required, were manufactured five sixlens interferometers on the same Si chip. All interferometer sets have fixed focal distance (z_f = 4 cm) that was achieved by varying the numbers of individual lenses in each lens array. All sets taken together allow covering considerable X-ray energy range from 10 to 50 keV. To choose the desirable working energy, one can switch from one interferometer set to another by parallel displacement of the chip in vertical direction. Table 1 summarized the main parameters of the sixlens sets.

Table 1. Parameters of the sixlens interferometers.

Set number	Energy	Number of lenses	Total lens length, μm	Diffraction limited resolution, nm*	Effect. aperture, μm
1	10	10	618	190	13
2	20	39	2416	87	17
3	30	87	5392	63	21
4	40	156	9670	55	23
5	50	243	15064	53	23

* Diffraction limited resolution calculated for single lens array in the interferometer

3. THEORY

We have elaborated a computer program with the aim to simulate optical properties of X-ray multilens interferometer. The program is performed on the base of general theory of X-ray phase contrast imaging [25]. The wave field of radiation from the point source at the distance z_0 is described by $\exp(iKz)P(x, z_0)$, where

$$P(x,z) = \frac{1}{(i\lambda z)^{1/2}} \exp(i\pi \frac{x^2}{\lambda z}), \quad (1)$$

is the Fresnel propagator which is, in fact, a part of spherical wave in the paraxial approximation, $K = 2\pi/\lambda$, λ is the wavelength, x is a transverse coordinate and z is the coordinate along the optical axis. The exponential term $exp(iKz)$ can be omitted because it does not influence the intensity.

Let us consider the multilens interferometer, which consists of M arrays of CRLs separated by distance d. The length of the interferometer is much smaller than the distance to the source, therefore to study its optical properties we treat the interferometer as a phase object which can be taken into account by the transmission function

$$T(x) = exp(-iK\,[\delta - i\beta]t(x)), \quad (2)$$

where $t(x)$ is a variable thickness of the M-lens interferometer along the ray parallel to the optical axis. It is easy to calculate that $t(x)$ is a sum of terms; each of them is the thickness of one CRL

$$t_k(x) = N(x - x_k)^2 / R, \qquad x_k = d(k - \frac{M+1}{2}), \qquad k = 1, \ldots M, \quad (3)$$

where N is a number of individual lenses in CRL, R is a curvature radius, x_k is a position of the k-th lens center, M is a number of CRLs in the interferometer.

A propagation of the wave through free space on the distance z_1 between the interferometer and the detector is described by a convolution of wave function and $P(x, z_1)$. The total expression can be transformed to a new form as a product $P(x, z_t)$ and a convolution of $T(x)$ and $P(x, z_r)$, where $z_t = z_0 + z_1, z_r = z_0 z_1 / z_t$. Then a relative intensity is calculated as follows

$$I(x) = \left|a(x_0)\right|^2, \quad a(x_0) = \int dx_1 P(x_0 - x_1, z_r) T(x_1), \qquad x_0 = x z_0 / z_t \tag{4}$$

We note that if z_0 is not large compared to z_1 then the image becomes increased compared to object, however, all features of the image stay the same.

On the basis of the formulae presented above we developed the computer program which allows performing numerical simulation of the optical properties of the multilens interferometer for diverse parameters of the experimental setup. The finite size of the source was taken into account by a calculation of the convolution of the intensity for a point source and Gaussian with FWHM as $S(z_1/z_0)$ where S is the source size.

Nevertheless, the general properties of multilens interferometer can be formulated without calculations. It is of interest to analyze the main features of the interference fringes analytically. It is known that the M-lens interferometer transforms the incoming parallel beam to M-set of divergent beams behind the focusing distance z_f. We will assume symmetrical case with M being even. These focal lines are placed periodically in space along the axis x with the period d. Our goal is to determine the distances z_n where rays from all sources come to the optical axis ($x = 0$) with the same phase or with a difference which is integer number of 2π. It is clear that the relative intensity will be increased from 1 to M^2 at such distances. One can calculate the ray path r_k from k-th CRL to the optical axis at the distance z from the sources and consider a difference of ray paths for the arbitrary k and j sources. The result is

$$r_k - r_j = r_{kj}^{(0)} = \frac{d^2}{z}\left[(k-j)\left(\frac{k+j}{2} - \frac{M+1}{2}\right)\right] \tag{5}$$

Since k, j, M are integer and M is even the expression in the square brackets is integer. Indeed, if $(k - j)$ is odd then $(k + j)$ is odd too and the expression in the second round bracket is integer. If $(k - j)$ is even then the expression in the round bracket is semi-integer but it is multiplied by even integer.

Thus the condition for constructive interference of secondary sources produced by M CRLs of the interferometer can be written as $d^2/z = \lambda n$ where n is arbitrary integer number. Distance $z_T = 2d^2/\lambda$ is Talbot distance where the set of M periodic line sources are reproduced. Halfway through the picture, a secondary Talbot image is formed which shifted vertically from the primary image by half a period. At distances $z_n = d^2/(\lambda n) = z_T/2n$ between primary and secondary Talbot images the shrunken fractional Talbot images can be observed.

The next step is to calculate the period of the interference fringes. We repeat all calculations for the point having x coordinate and obtain the result for the distances z_n as follows

$$r_k - r_j = r_{kj}^{(0)} - \frac{xd}{z_n}(k-j) = r_{kj}^{(0)} - \lambda n \frac{x}{d}(k-j) \tag{6}$$

This expression shows that the period of interference fringes is $\Lambda = d/n$. The case $M = 2$ is specific because the expression in the square brackets of eq. (5) is equal to zero, therefore the high contrast, sharp interference pattern exist at any distance. Correspondingly, the period depends directly on the distance and is equal to $\Lambda = \lambda z/d$.

Let us now estimate the width w_t of the interference fringe maximum across the beam. We will assume that the distance z is sufficiently large and all CRLs can interfere. In this case we can replace each secondary source by the real point source which is described by the function $P(x, z)$. Then intensity can be written as $I(x,z) = (\lambda z)^{-1} K_f(x,z)$. Initially the function $K_f(x,z)$ is a sum of M and a double sum of cosines of complex argument which contains coordinates of all CRLs. The double sum can be reordered to a more suitable expression which can be simplified significantly in the case of $z = z_n$.

We omit calculations and present the result

$$K_f(x,z_n) = M + 2\sum_{m=1}^{M-1}(M-m)\cos\left(2\pi\frac{m}{\Lambda}x\right), \quad \Lambda = \frac{d}{n} \tag{7}$$

We note that this expression is valid for the finite M secondary sources produced by interferometer, while the Talbot effect is applicable for the infinite periodic system. The period of the fringes does not depend on M; whereas the fringe intensity of the interference pattern is determined by M. For $x = 0$ we have $K_f(0,z_n) = M^2$, at the same time a mean value of the fringe intensity averaged over the fringe period is equal to M.

To estimate a peak width we note that a numerical calculation of $K_f(x,z_n)$ shows that for large M it is a peak which can be described approximately by Gaussian $K_f(x) \approx M^2 exp(-\alpha x^2)$. We can calculate the parameter α from the first term of the expansion of (7) in power series. As a results we have

$$\alpha = \left(\frac{2\pi}{\Lambda}\right)^2 \frac{M^2-1}{12}, \quad w_t = \frac{1.665}{\alpha^{1/2}} = \Lambda\frac{0.918}{(M^2-1)^{1/2}} \tag{8}$$

One can see that for bilens interferometer $M = 2$ we have $w_t = 0.52\Lambda$ whereas $w_t = 0.92\Lambda/M$ for large values of M.

To estimate a peak depth we can put $x = 0$ and consider $z = z_n(1+s/n)$. Considering the general expression in this particular case and making a replacement of variable one can obtain

$$K_{1f}(0,s) = M + 2\sum_{m=1}^{M-1}\sum_{l=-(M-m-1)/2}^{(M-m-1)/2}\cos(2\pi mls) \tag{9}$$

Now we apply the same procedure as above and expand the function over s. The first two terms of expansion are

$$K_{1f}(0,s) = M^2 - (2\pi s)^2 C, \quad C = \sum_{m=1}^{M-1} m^2 \sum_{l=-(M-m-1)/2}^{(M-m-1)/2} l^2 = \frac{M^2(M^2-1)(M^2-4)}{720} \tag{10}$$

The calculation is cumbersome but a physical meaning is evident because C must be equal zero for $M = 0, 1, 2$.

Now it is easy to calculate w_l as follows

$$w_l = \frac{d^2 w_s}{\lambda M^2} \approx \frac{7.111\Lambda^2}{\lambda M^2} \approx 8.438\frac{w_t^2}{\lambda}, \tag{11}$$

where w_s is FWHM for the function (10). We note that the relation between w_l and w_t is very similar to the same relation for the focus spot and differs only by numerical coefficient 8.438 instead of 7.850. It proves once again that Talbot effect is focusing.

4. EXPERIMENT AND RESULTS

The experimental tests of the sixlens interferometer were performed at the Micro Optics Test Bench (MOTB) of the ID06 ESRF beamline. A liquid nitrogen cooled Si-111 double crystal, fixed exit monochromator was used to adjust the X-ray energy in the range 10 - 30 keV. The sketch of the experimental setup is shown in Fig.2. The Si sixlens system was mounted at a distance z_0 = 56 m from the source. Interference patterns were recorded with the high resolution x-ray CCD camera with a spatial resolution about 1.3 μm (0.65 μm pixel size).

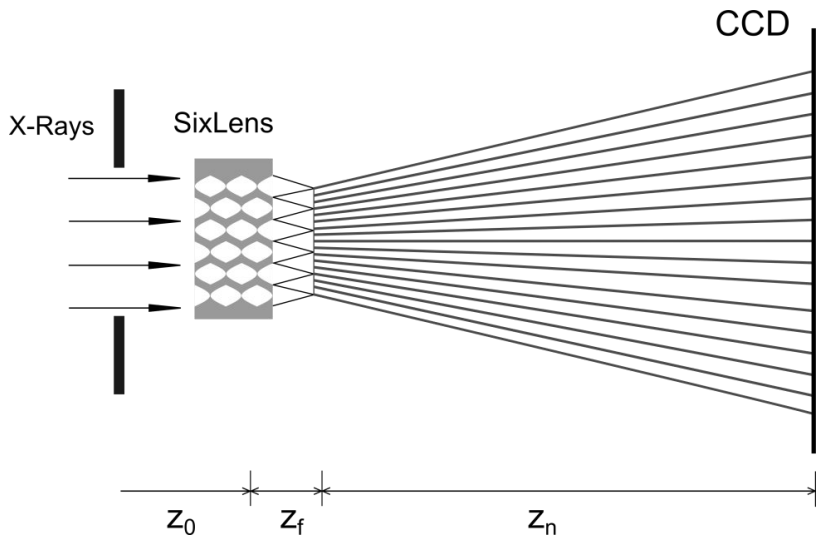

Figure 2. Schematic view of sixlens interferometer.

To record the interference pattern at the fractional Talbot distances, the CCD camera was placed at the distance $z_1 = z_f + z_n$ from the interferometer. The typical exposure time was 2 seconds during a 7/8 beam bunch mode (200 mA current). The quality of the fringes produced by a multilens system can be described quantitatively using the visibility $V = (I_{\max} - I_{\min}) / (I_{\max} + I_{\min})$, where I_{max} and I_{min} are the irradiances corresponding to the maximum and nearby minimum in the fringe system, respectively. In view of the fact that distance z_0 is much larger than expected observation distance, it is possible to use the plane wave approximation, considering the parameters of sixlens interferometer it can be easily estimated that for 12 keV X-rays the Talbot distance z_T is in the order of 18 m. Taking into account the beamline characteristics (energy range, length) and CCD spatial resolution to resolve interference fringes, the fractional p/q = 1/6 Talbot image was chosen for interferometer characterization. Using the formula to calculate an observation distance $z_n = \frac{1}{6} z_T$, the distance for fractional Talbot image is around 3 m. It should be noted that calculated observation distance for spherical wave approximation is only 6 cm larger. The observed interference pattern and intensity variation obtained for the line through the center (cross section) of the fringe pattern are shown in Fig. 3. The fringes are visible vertically up to few millimeters. The measured fringe spacing was Λ = 10.3 μm, which is in good agreement with calculations. The measured FWHM of the fringe maximum is 3 μm, while according to the calculations it should be around of 1.7 μm. The broadening of the measured fringe width is caused by the finite size of the source. Numerical calculations of interference patterns with varying of source size had shown compliance 3 μm peak FWHM to source size S = 40-50 μm. The spatial coherence length described $l_{coh} = \lambda z_0 / S$, where S is a source size, is in the order of 130 μm while the total width of interferometer is 180 μm. Based on numerical calculations it can be concluded : only 4-5 lens arrays were located under coherent illuminations.

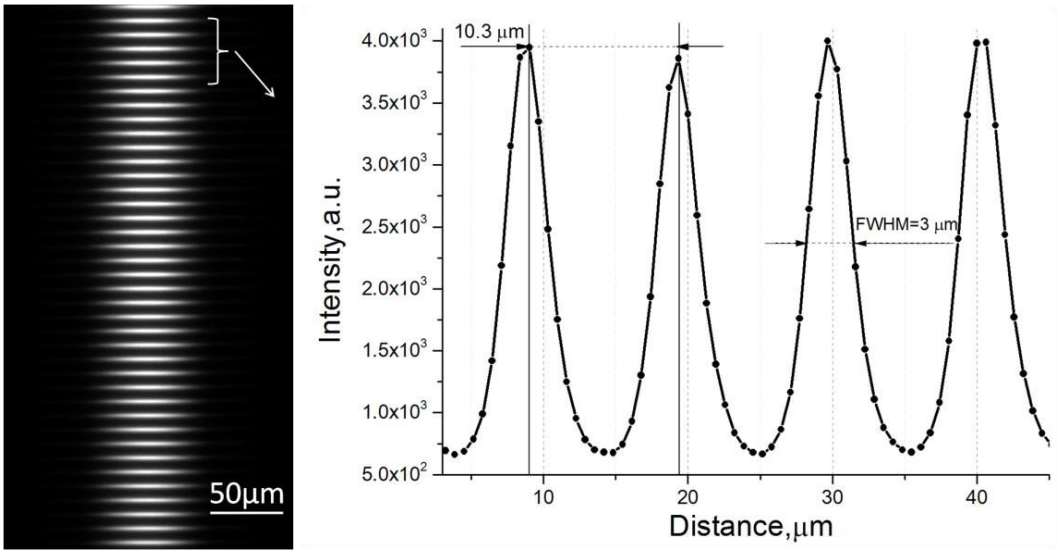

Figure 3. An interference pattern (left) generated by a sixlens system, recorded at a 1 Å wavelength. The intensity variation (right) obtained for the line though the centre of the fringe pattern.

To demonstrate the interference fringe maximum narrowing in the case of the sixlens interferometer, the interference pattern produced by bilens interferometer was recorded under the identical experimental conditions in terms of energy and distances: 12 keV and 3 m respectively. Bilens interferometer consists of two lens arrays with the separation period of 30 μm. The measured fringe spacing (peak-to-peak distance) of bilens interference pattern was 10.3μm. The comparison of the intensity variation through the center of fringe pattern for bilens and sixlens interferometers is shown in Fig 4. The measured FWHM of fringe maxima for bilens interferometer is 5.2 μm, as for sixlens interferometer it is 3 μm. The results show a narrowing of the interference fringes but unfortunately not as much as we expected. As it was discussed above, the reason for this is a finite source size and partial coherent illumination. Therefore it is clearly seen that the contrast of the fringes produced by sixlens interferometer is superior to fringe contrast after bilens.

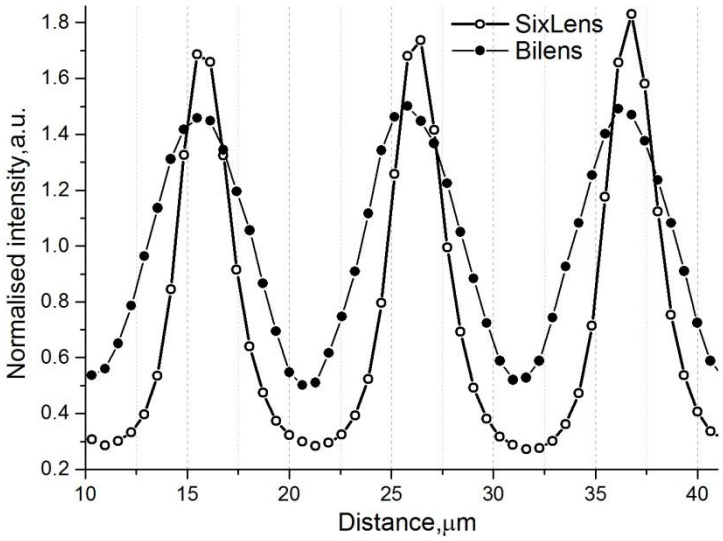

Figure 4. The comparison of interference fringes produced by bilens (filled points) and multilens (open points) systems.

Let us estimate how stable the interference picture in terms of depth of field (DOF) is. We tested DOF for sixlens interferometer at energy E = 12 keV and we define it as a range of distances along the optical axis of the interferometer trough which the visibility of the interference pattern decreases by a factor of two. For this we placed the chip at distance of 1/12 fractional Talbot image, which was around 1.5 meters. The fringe period at this distance is 5 μm and FWHM of the fringe maximum is 1.5 μm. The interferometer was scanned along the optical axis ± 5 cm around exact position with the 1 mm step. At each position the interference pattern was registered and visibility of the fringes was measured. The result is presented in Fig. 5. It is clearly seen that DOF is in the order of 5 cm. This value is in very good agreement with calculation by the program. Let us consider the sixlens interferometer at p/q = 1/300 Talbot distance with the fringe periodicity 200 nm and FWHM of the fringe maximum 40 nm. In this case the interferometer depth of field is 130 microns. It should be noted that under the same conditions for the Si nanolenses with the FWHM focal spot of 40 nm, the depth of focus will be only 10 microns.

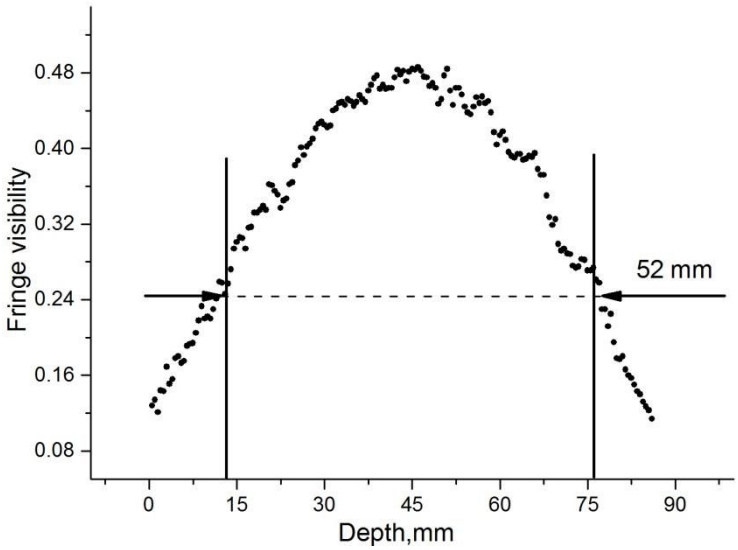

Figure 5. The depth of field of 1/12 fractional Talbot image.

The sixlens interferometer was tested with 24 keV X-rays and interference pattern (cross-section is presented on Fig. 6) was registered at fractional Talbot p/q = 1/12 image distance which is z_n = 3 m. Experimentally measured fringe spacing of recorded interference pattern was 6.3 μm and FWHM of the fringe maximum was 2.7 μm. The measured contrast was around 40%. We did not observe the expected fringe width contraction and it can be explained by the fact that at higher energies the spatial coherence length decreasing: it can be easily estimated, by the formula presented above, that at 24 keV the coherence length is in the order of 70 μm. This means that at least 3 arrays are illuminated coherently, which leads to the broadening of the interference fringes and decreasing of the fringe visibility.

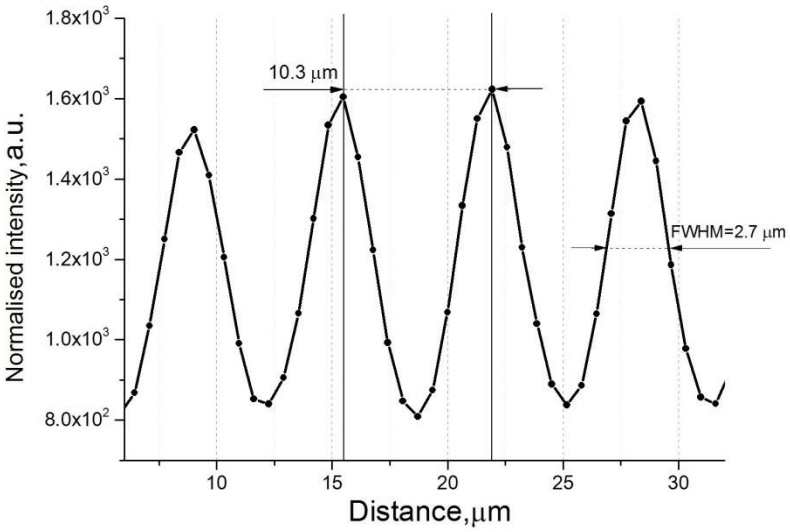

Figure 6. The cross section of interference pattern produced by sixlens system under 24 keV illumination.

Sixlens interferometer was also experimentally tested with the point source produced by Si planar refractive lenses. The lens consists of 26 individual lenses with radius of parabola apex of 6.25 μm and aperture 50 μm. At energy E = 12 keV it has a focal distance z_{f1} = 3.5 cm. The Si lens was located at z_{01} = 55 m from the source. The interferometer was placed at z_0 = 50 cm distance from the secondary source, see Fig. 7.

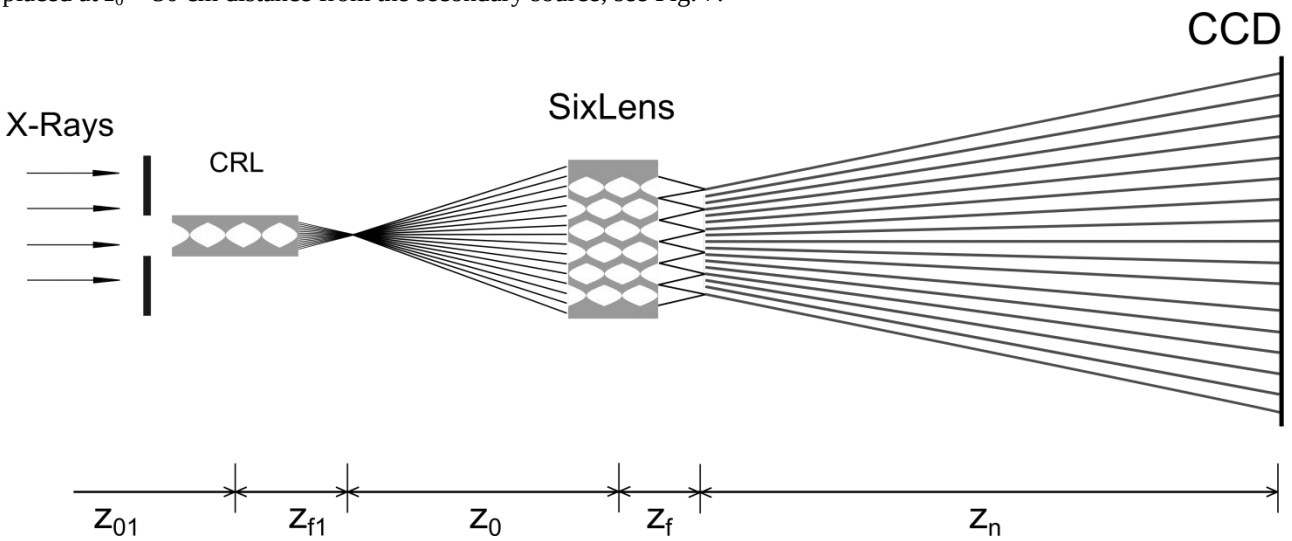

Figure 7. Experimental set-up of the experiment with secondary source.

In the case when incident radiation comes from a point source at a finite distance z_0 the spherical wave approximation has to be considered. It is readily shown that Talbot distance will be magnified by a factor $(z_n + z_0 + z_f)/z_0$ and interference occurred at distance z_n given by:

$$\frac{1}{z_f + z_n} + \frac{1}{z_0} = \frac{1}{z_f^{(\infty)} + z_n^{\infty}}, \quad z_f^{\infty} = \frac{R}{2\delta N}, \quad z_n^{\infty} = \frac{d^2}{\lambda n}, \quad z_f = \frac{z_f^{\infty}}{1 - z_f^{\infty} / z_0} \tag{12}$$

Fractional Talbot image p/q = 1/40 was registered at distance z_n = 3.8 m from the interferometer, cross section is presented on Fig.8. Fringe spacing is 11.5 μm and FWHM of the interference fringe maximum is 3.1 μm. The measured visibility of the interference pattern is 91.5% (calculated 93%), which correspond to the secondary source in the order of 220 nm. It should be mentioned that for the plane wave illumination the fractional p/q = 1/40 Talbot image is at 45 cm distance from the interferometer. The period of the fringe pattern is 1.5 μm and an FWHM fringe maximum is 0.25 μm that is very difficult to resolve with our camera.

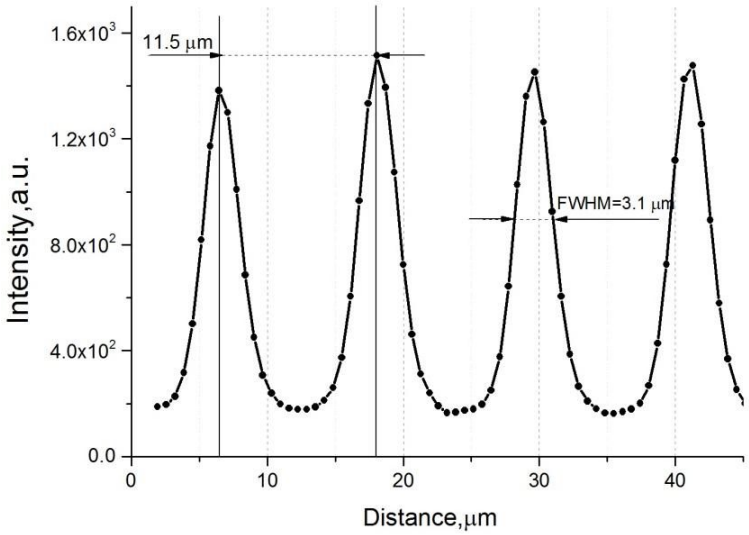

Figure 8. The cross section of interference pattern recorded in the experiment with secondary source.

4. CONCLUSIONS

A sixlens interferometer as a chessboard pattern of the lens arrays was designed and manufactured for hard X-rays. The sixlens interferometer was studied at the energy range from 10 to 30 keV. The interference fringe images were recorded at different fractional Talbot distances. Narrowing of the interference fringe width produced by sixlens system was confirmed experimentally by comparison with the bilens interferometer. The enhancement of the fringe contrast was observed as well. The depth of field was investigated and it is shown that it changed with the fraction of Talbot distance. Even at p/q = 1/40 fractional Talbot distance the depth of field for sixlens interferometer is more than 10 times greater compared with Si nanolens with the same focal spot. More than 90% interference fringe contrast produced by the multilens interferometer under point source illumination demonstrates sufficient quality of the sixlens interferometer structure.

The possibility to generate an interference pattern in paraxial geometry may be used in a standing wave technique [26]. The strong sensitivity to optical distortions of the beamline gives possibility to use the interferometer for optics diagnostics and coherence characterization A coherent illumination provided by the interferometer can be used for studies of mesoscopic photonic crystals by a moiré-like radiography and phase contrast imaging, as a classical interferometer. In addition, the proposed interferometer can be applied for electrochemical X-ray photolithography resulting in a direct non-contact pattern transfer onto an electrodeposited metal film [27].

It should be noted that the six–lens system can be easily extended to an mm-size aperture multilens interferometer which is comparable with the beam size at the ESRF undulator beamlines.

ACKNOWLEDGMENTS

The authors are very grateful to C. Detlefs for his help and support during the experiments at ID 06 beamline. The work was supported by the Ministry of Science and Education of Russian Federation (grants № 14.Y26.31.0002, № 02.G25.31.0086, and project 8364) and RFBR grant № 13-02-00469.

REFERENCES

[1] Leitenberger, W., Kuznetsov, S. M. and Snigirev, A., "Interferometric measurements with hard X-rays using a double slit," Opt. Commun. 191, 91-96 (2001).

[2] Fezzaa, K., Comin, F., Marchesini S., Coïsson, R., and Belakhovsky, M., "X-Ray Interferometry at ESRF Using Two Coherent Beams from Fresnel Mirrors," J. Xray Sci. Technol. 7(1), 12-23 (1997).

[3] Momose, A., Kawamoto, S., Koyama, I., Hamaishi, Y., Takai, K., Suzuki, Y., "Demonstration of X-Ray Talbot Interferometry," Jap. Jour. Appl. Phys. 42, 866 (2003).

[4] Snigirev, A., Kohn, V., Snigireva, I. and Lengeler, B., "A compound refractive lens for focusing high-energy X-rays," Nature 384(6604), 49-51 (1996).

[5] Lengeler, B., Schroer, C. G., Richwin, M., Tümmler, J., Drakopoulos, M., Snigirev, A. and Snigireva, I., "A microscope for hard x rays based on parabolic compound refractive lenses," Appl. Phys. Lett. 74, 3924 (1999).

[6] Lengeler, B., Schroer, C., Tummler, J., Benner, B., Richwin, M., Snigirev, A., Snigireva, I. and Drakopoulos, M., "Imaging by parabolic refractive lenses in the hard X-ray range," J. Synchrotron Radiat. 6(6), 1153-1167 (1999).

[7] Aristov, V., Grigoriev, M., Kuznetsov, S., Shabelnikov, L., Yunkin, V., Weitkamp, T., Rau, C., Snigireva, I., Snigirev, A., Hoffmann, M. and Voges, E., "X-ray refractive planar lens with minimized absorption," Appl. Phys. Lett. 77(24), 4058-4060 (2000).

[8] Schroer, C. G., Kurapova, O., Patommel, J., Boye, P., Feldkamp, J., Lengeler, B., Burghammer, M., Riekel, C., Vincze, L., van der Hart, A. and Küchler, M., "Hard x-ray nanoprobe based on refractive x-ray lenses," Appl. Phys. Lett. 87(12), 124103 (2005).

[9] Snigirev, A., Snigireva, I., Grigoriev, M., Yunkin, V., Di Michiel, M., Kuznetsov, S. and Vaughan, G., "Silicon planar lenses for high-energy x-ray nanofocusing.," Proc. SPIE 6705, 670506 (2007)

[10] Kohn, V., Snigireva, I. and Snigirev, A., "Diffraction theory of imaging with X-ray compound refractive lens," Opt. Commun. 216, 247-260 (2003).

[11] Schropp, A., Hoppe, R., Patommel, J., Samberg, D., Seiboth, F., Stephan, S., Wellenreuther, G., Falkenberg, G. and Schroer, C. G., "Hard x-ray scanning microscopy with coherent radiation: Beyond the resolution of conventional x-ray microscopes," Appl. Phys. Lett. 100(25), 253112 (2012).

[12] Drakopoulos, M., Snigirev, A., Snigireva, I., and Schilling, J., "X-ray high-resolution diffraction using refractive lenses," Appl. Phys. Lett. 86,014102 (2005).

[13] Petukhov, A. V., Thijssen, J. H. J., Hart, D. C. t., Imhof, A., Blaaderen, A. v., Dolbnya, I. P., Snigirev, A., Moussaid, A. and Snigireva, I., "Microradian X-ray diffraction in colloidal photonic crystals," J. Appl. Cryst. 39, 137-144 (2006).

[14] Bosak, A., Snigireva, I., Napolskii, K. S. and Snigirev, A., "High-Resolution Transmission X-ray Microscopy: A New Tool for Mesoscopic Materials," Adv. Mater. 22(30), 3256-3259 (2010).

[15] Ershov, P., Kuznetsov, S., Snigireva, I., Yunkin, V., Goikhman, A. and Snigirev, A., "Fourier crystal diffractometry based on refractive optics," J. Appl. Cryst. 46(5), 1475-1480 (2013).

[16] Snigirev, A., Snigireva, I., Kohn, V., Yunkin, V., Kuznetsov, S., Grigoriev, M. B., Roth, T., Vaughan, G. and Detlefs, C., "X-Ray Nanointerferometer Based on Si Refractive Bilenses," Phys. Rev. Lett. 103(6), 064801 (2009).

[17] Talbot, H. F., "LXXVI. Facts relating to optical science. No. IV," Phil. Mag. Series 3 9(56), 401-407 (1836).

[18] Rayleigh, L., "XXV. On copying diffraction-gratings, and on some phenomena connected therewith," Phil. Mag. Series 5 11(67), 196-205 (1881).

[19] Patorski, K., "I The Self-Imaging Phenomenon and its Applications," Progress in Optics E. Wolf ed.1, 1-108 (1989)

[20] Winthrop, J. T. and Worthington, C. R., "Theory of Fresnel Images. I. Plane Periodic Objects in Monochromatic Light," J. Opt. Soc. Am. 55(4), 373-380 (1965).

[21] Cowley, J. M. and Moodie, A. F., "Fourier Images IV: The Phase Grating," Pro. Ph. So. 76(3), 378-384 (1960).

[22] Hartman, Ya.M. and Snigirev, A., "Some examples of high energy X-rays phase contrast," X-ray Microscopy 4, 429–432 (1994)

[23] Weitkamp, T., Diaz, A., David, C., Pfeiffer, F., Stampanoni, M., Cloetens, P. and Ziegler, E., "X-ray phase imaging with a grating interferometer," Opt. Express 13(16), 6296-6304 (2005).

[24] Cloetens, P., Guigay, J. P., De Martino, C., Baruchel, J. and Schlenker, M., "Fractional Talbot imaging of phase gratings with hard x rays," Opt. Lett. 22(14), 1059-1061 (1997).

[25] Snigirev, A., Snigireva, I., Kohn, V., Kuznetsov, S. and Schelokov, I., "On the possibilities of x-ray phase contrast microimaging by coherent high-energy synchrotron radiation," Rev. Sci. Instrum. 66 (12), 5486-5492 (1995).

[26] Zegenhagen, J., "Surface structure determination with X-ray standing waves," Surf. Sci. Rep. 18, 202-271 (1993).

[27] Eliseev, A. A., Sapoletova, N. A., Snigireva, I., Snigirev, A. and Napolskii, K. S., "Electrochemical X-ray Photolithography," Angew. Chem. Int. Ed. 51(46), 11602-11605 (2012).